JOURNAL OF APPLIED ELECTROCHEMISTRY **28** (1998) 503–510

Copper removal during formation of corrosion resistant alkaline oxide coatings on Al–Cu–Mg alloys

R. G. BUCHHEIT

Mechanical Metallurgy and Corrosion Department, Sandia National Laboratories, Albuquerque, New Mexico 87185, USA

Received 30 December 1996; revised 15 July 1997

The performance of corrosion resistant inorganic oxide coatings formed on Al–Cu–Mg alloys is often degraded by Cu enrichment that occurs during oxide formation. This is particularly true of coating processes conducted in basic solutions. A modification to an alkaline oxide coating process has been made that simultaneously eliminates Cu enrichment and forms a corrosion resistant coating. In this paper, the modified process is described and the resulting coating morphology, structure and composition are reported. Results from electrochemical and exposure corrosion tests show that useful gains in corrosion resistance are achieved. Cu removal during the modified process is rationalized using an argument based on the increase in Cu solubility that occurs in solutions with a pH greater than the solubility minimum for Cu (9.8), and the effect of Cu complexing by carbonate.

Keywords: *copper*, *alloy*, *copper enrichment*, *copper removal*

1. Introduction

Copper is an important alloying element in commercial aluminium alloys. Copper additions to aluminium, usually in combination with other elements, enable a desirable mix of mechanical properties to be developed through natural and artificial ageing practices. Up to 6.5 wt % Cu is added to wrought heat treatable alloys [1], and up to 14 wt % is added to cast alloys [2]. In binary alloys, the solid solubility of Cu varies from approximately 5.7 wt % at the solidus temperature to 0.05 wt % at room temperature [3]. Cu solubility is sometimes lowered when other alloying elements are present. As a result, much of the copper added to an alloy is segregated into second phase particles.

In many aqueous surface finishing procedures, the presence of Cu in aluminium is problematic. During finishing, the surfaces of work pieces become enriched with a variety of copper compounds, occasionally including metallic Cu, that are collectively referred to as 'smut'. Cu smut forms in etching alkaline degreasing solutions where Cu solubility is low [4]. Less frequently, it is observed to accumulate on surfaces during deoxidizing where aggressive chemical action intended to remove surface oxides attacks the underlying alloy substrate [5]. Metallic copper deposits form because the open circuit potential for the alloy substrate is negative to the reduction potential for Cu (how Cu is liberated from the alloy to begin with has not yet been explained for all relevant environments). Cu smut interferes with conversion coating formation [6], anodization [7] and with bonding of subsequently applied adhesives and paints [6, 8, 9]. It is also suspected to contribute to increased susceptibility to corrosion during service due to galvanic coupling with Cu-rich surface regions.

In aqueous solutions it is thermodynamically possible to use chemical or electrochemical oxidation to remove Cu from aluminium alloy surfaces. It is also possible to use Cu complexing agents to supplement the efficacy of Cu removal by Cu oxidation. Several techniques have been explored experimentally with some success [10]. These techniques have been carried out in advance of conversion coating or anodizing. However, Cu enrichment can occur during the subsequent coating formation processes. It does not appear likely that Cu removal can be achieved after an anodized or conversion coated surface has been formed without degrading corrosion resistance.

A possible remedy to this dilemma is to simultaneously remove Cu while forming the corrosion resistant coating. This has been implemented in a modification to an alkaline oxide coating process that results in the formation of a corrosion resistant coating consisting predominantly of hydrotalcite, $Li_2[Al_2(OH)_6]_2{\cdot}CO_3{\cdot}_3H_2O$. These coatings are uniform and do not contain Cu in excess of the nominal Cu content of the alloy substrate. Coatings formed on 2024-T3 (Al–4.4Cu–2.5Mg–0.6Mn) using this method exhibit no pitting after 168 hours of salt spray exposure. This level of performance is comparable to that of corrosion resistant grade chromate conversion coatings.

In this paper the modified hydrotalcite coating process is described. The resulting coating morphology, structure and composition are reported for the original hydrotalcite coating process and for the

0021-891X

modified process. Results from electrochemical corrosion testing and standardized salt spray exposure corrosion testing are presented. Last, the phenomenon of Cu removal during coating formation is rationalized using data reported in the literature for Cu solubility and Cu complexing by carbonate.

2. Experimental procedures

2.1. *Materials and surface preparation*

Aluminium alloy samples 100 mm × 125 mm × 2 mm thick were prepared from 2024-T3 (Al–4.4Cu–2.5Mg–0.6Mn) sheet stock and were used for all experiments. In the T3 temper, the alloy is naturally aged for a minimum of 30 days. Copper is segregated into a variety of second phase particles and is also retained in solid solution.

Mill finish surfaces were prepared for coating by washing in an aqueous alkaline detergent solution to remove paint, grease and dirt. Samples were then immersed in a nonetching sodium silicate–sodium carbonate solution at 65 °C for 2 min to remove any additional hydrocarbon contamination. Surface deoxidation was performed by immersion in a commercially available nitric acid–sodium bromate solution at 50 °C for 2 min [11]. Hydrotalcite coating formation was conducted by immersing samples in a solution comprised of 7.2 g dm^{-3} lithium carbonate, Li_2CO_3, plus 0.4 g dm^{-3} sodium aluminate, $NaAlO_2$, pH 11.5 for 15 min. At this point, some of the panels were set aside and allowed to air dry in advance of further testing. The remaining samples were then immediately immersed in a solution containing 7.2 g dm^{-3} Li_2CO_3; 7.4 g dm^{-3} lithium hydroxide, LiOH; and 4 g dm^{-3} $NaAlO_2$ at 55 °C for 180 min. This second solution had a pH of approximately 13.5. Samples were rinsed with flowing deionized water in between each processing solution. After processing, these samples were also allowed to dry in air at ambient temperatures. Samples exposed to the first solution only were prepared according to the original hydrotalcite formation process. Samples exposed to both solutions were prepared according to the modified process.

2.2. *Characterization of surfaces*

The morphology of sample surfaces was examined using scanning electron microscopy (SEM) carried out on an Amray 1645 scanning electron microscope. Grazing incidence angle X-ray diffraction (GIXRD) was used to identify compound present in surface films formed during exposure. Samples were examined using a Siemens D500 diffractometer at a grazing incidence angle of 4°. At this angle, the target sampling depth was approximately 1.0 μm. Auger electron spectroscopy (AES) and ion etching were used to generate sputter depth composition profiles for elements of interest. AES was conducted using a Physical Electronics PHI 660 scanning auger microprobe. Sputtering was conducted using a rastered 3 kV Xe^+ ion beam. Individual element signals were corrected using the appropriate sensitivity factors to generate semiquantitative composition against depth profiles.

2.3. *Corrosion testing of coated surfaces*

The corrosion resistance of coated surfaces was evaluated using electrochemical impedance spectroscopy (EIS) and salt spray exposure testing. EIS was conducted on coated surfaces exposed to 0.5 M NaCl solution exposed to ambient laboratory air. Measurements were initiated after 24 ± 1 h of exposure. Measurements were made using a three electrode arrangement (saturated calomel electrode as reference) in a flat cell that exposed 20 cm^2 of working electrode area. The cell was controlled using a Princeton Applied Research model 273 potentiostat and a Solartron 1255 frequency response analyser controlled by a commercially available software package [12]. EIS spectra were collected over a frequency domain ranging from 10 kHz to 10 mHz using a 10 mV amplitude sinusoidal voltage perturbation. Spectra were collected at a rate of 10 points per decade frequency. EIS data were fitted to an equivalent circuit model using a complex nonlinear least squares fitting routine to extract coating resistances and capacitances.

Salt spray testing was conducted for 168 h per ASTM B117 [13] which specifies exposure of coated panels at 35 °C (95 °F) to a fog generated by atomizing a 5% NaCl solution and injecting it into an enclosed exposure chamber. After exposure, samples were rinsed in deionized water and visually inspected for evidence of corrosion damage.

3. Results

3.1. *Hydrotalcite coating*

Degreasing and deoxidizing procedures were carried out prior to coating to remove organic debris and surface oxide films. Sample surfaces exhibited a dull metallic finish indicating very slight etching during deoxidation. Upon immersion in to the pH 11.5 Li-salt solution, vigorous hydrogen evolution occurred and a black to grey surface film developed. Hydrogen evolution ceased within 2 min of initial exposure although samples were immersed for a total of 15 min. A group of samples were removed and withheld from further processing and retained for surface analysis and corrosion testing, the remainder were further processed by exposure to the pH 13.5 Li-salt solution. Upon immersion in this solution, samples once again evolved hydrogen at a moderate to slow rate for a period of up to 5 min. The surface then changed colour from black or grey to green/yellow and eventually cleared leaving a white translucent coating. The colour transformation was complete within 60 min although samples were immersed in this solution for a

total of 180 min. In all cases the coatings formed were thin and adherent to the alloy substrate.

3.2. *Surface characterization*

Surfaces of samples from each group were examined by SEM, grazing incidence X-ray diffraction (GI-XRD), and auger electron spectroscopy (AES). Figure 1 is a scanning electron micrograph of a 2024-T3 surface after exposure in the pH 11.5 Li-salt solution. The surface film is featureless except for cracks that probably formed as the film shrank during drying. Figure 2 shows the surface morphology after the additional 180 min exposure to the pH 13.5 Li-salt solution. In this case, the distinctive surface morphology associated with hydrotalcite coatings is observed [14]. The coating shown in Figure 2 is continuous across the surface and forms over Cu, Mg, and Fe-rich second phase particles present in the alloy. Figure 3 illustrates the continuity of the coating using a topology sensitive secondary electron imaging (SEI) mode. Figure 4 shows the same region imaged using a composition sensitive backscattered electron imaging (BEI) mode. This micrograph reveals the location of Cu and Fe-rich particles in the image frame of Figure 3. Comparison of Figs 3 and 4 shows that the coating forms without interruption over the solute-rich second phase particles.

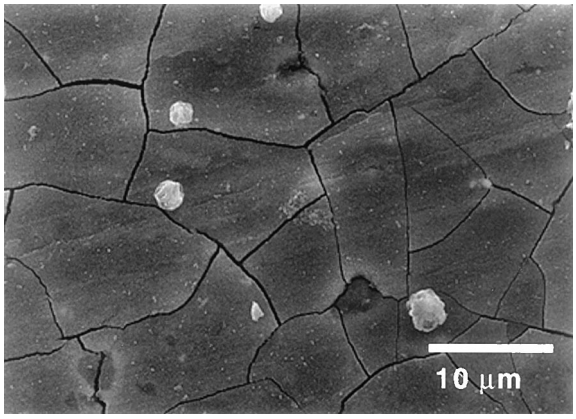

Fig. 1. SEM of a 2024-T3 surface after exposure to the pH 11.5 Li-salt solution for 15 min.

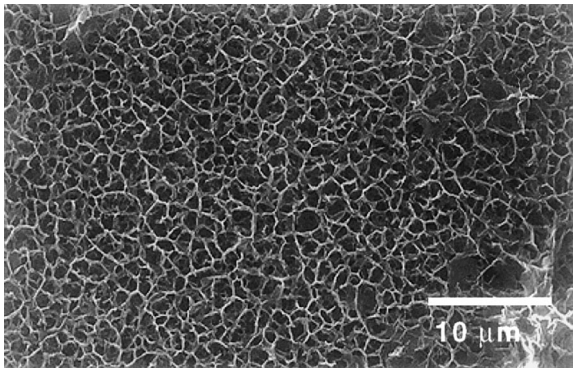

Fig. 2. SEM of a 2024-T3 surface after exposure to pH 11.5 Li-salt solution for 15 min followed by exposure to pH 13.5 Li-salt solution for 180 min.

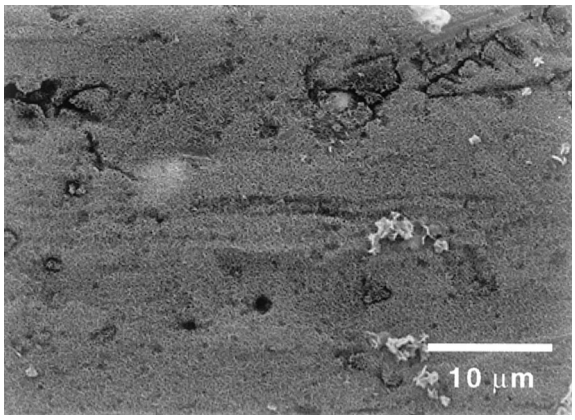

Fig. 3. SEI of 2024-T3 after exposure to pH 11.5 and 13.5 Li-salt solutions showing uniform coating coverage.

Figures 5 and 6 show oxygen, copper and aluminium sputter depth profiles for the surface of 2024-T3 with and without exposure to the pH 13.5 solution. Figure 5 shows the depth profiles for Al, O and Cu for a surface after exposure to the pH 11.5 solution. A Mg profile was also collected, but has been omitted for clarity. The surface film and substrate regions can be clearly distinguished by the sharp decrease in the oxygen signal and the corresponding increase in Al signal after 2000 s of sputtering time. The Cu profile exhibits a broad maximum with a peak concentration that is approximately four times the concentration present in the alloy substrate. As has been found in other studies, this maximum occurs near the oxide–metal interface [7]. It should be noted that there was also a maximum in the Mg profile at the same position noted for Cu. The level of peak Mg enrichment was also approximately four times that observed in the alloy substrate.

Figure 6 shows depth profiles after exposure to the pH 13.5 solution. As in Fig. 5, the oxide metal interface is reached after approximately 2000 s of sputtering indicating little or no net change in coating thickness during exposure to the pH 13.5 solution

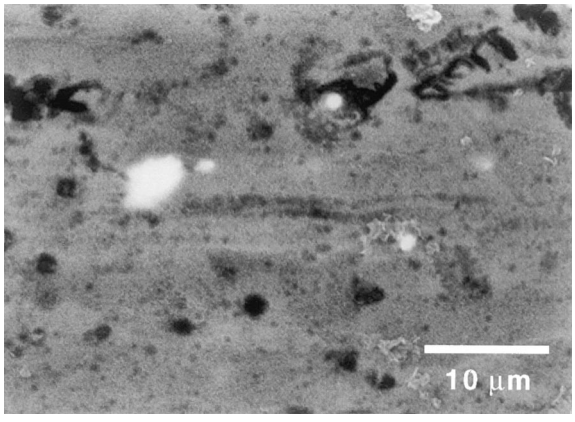

Fig. 4. BEI of the same region shown in Fig. 3 indicating the location of Cu, Fe, Mn-rich second phase particles (bright spots) covered by the coating.

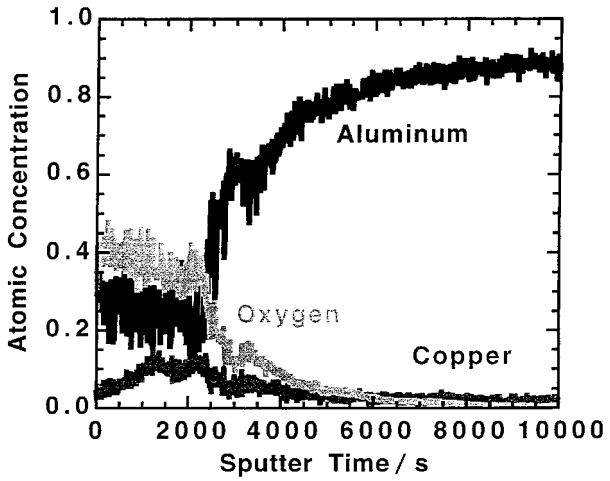

Fig. 5. Al, O and Cu sputter depth profiles from the surface film formed after exposure to the pH 11.5 solution.

assuming similar sputter rates for each oxide film. In this case, the maximum in the Cu concentration profile is absent showing that exposure to this solution removes Cu from the coating. The maximum in the Mg concentration profile detected after pH 11.5 exposure was also eliminated.

Figure 7 shows GIXRD patterns for 2024-T3 surfaces with and without exposure to the pH 13.5 Li-salt solution. The lower pattern is from the surface exposed to the pH 11.5 solution. This pattern contains the major reflections for aluminium from the underlying substrate (at 38° and 44° 2θ) and for $Al(OH)_3$ as bayerite which is present in the surface coating. The pattern also contains reflections near 30° 2θ that could not be conclusively indexed. The upper GIXRD pattern is from a surface after exposure to the pH 11.5 solution and the pH 13.5 solution. Aluminium and bayerite reflections are again observed. Additional reflections due to hydrotalcite are observed. The unindexed reflections near 30° in the lower pattern are now absent suggesting that they were associated with a Cu or Mg-containing compound that was removed during exposure to the pH 13.5 solution.

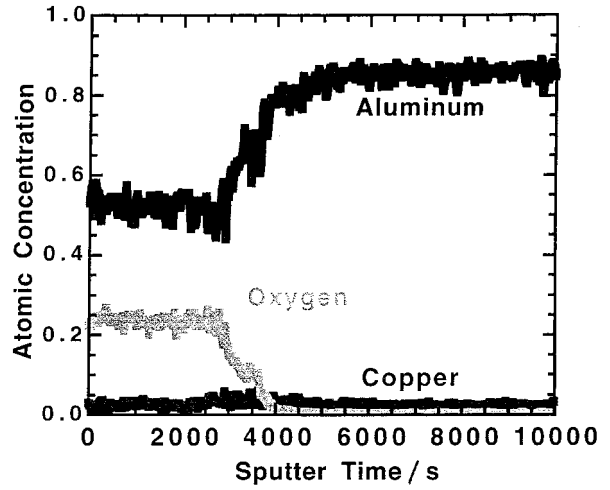

Fig. 6. Al, O, and Cu sputter depth profiles from the surface film formed after exposure to the pH 11.5 and 13.5 Li-salt solutions.

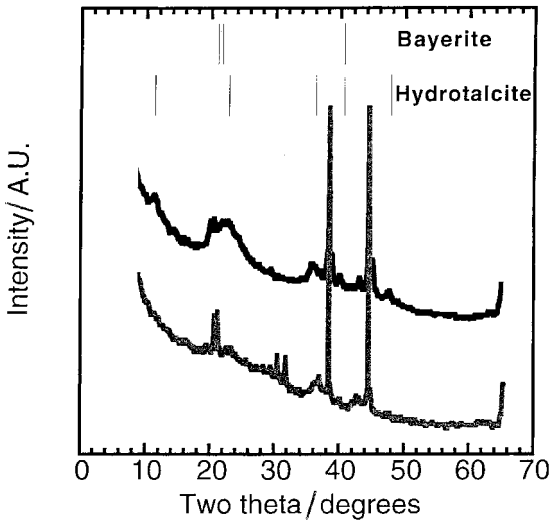

Fig. 7. GIXRD patterns from surfaces of 2024-T3 exposed to pH 11.5 solution (lower) and both the pH 11.5 and 13.5 solutions (upper). Uppermost hashes indicate locations of major bayerite and hydrotalcite reflections.

Coating thicknesses were not directly measured in these experiments. However, based on prior work, it is known that the hydrotalcite films formed on 99% pure Al in a pH 13.5 solution are 3 to 5 μm thick [4]. These thicknesses are appropriate estimates for the coatings formed in these experiments.

3.3. *Corrosion resistance*

In both electrochemical and salt spray exposure corrosion testing, the results of which are described below, corrosion resistance increased in the order: uncoated < coated in pH 11.5 solution $\ll$ coated in pH 11.5 and 13.5 solutions. The corrosion resistance of the samples treated in both solutions was great enough that no pitting was observed after 168 h of salt spray exposure. Bare surfaces and surfaces coated in the pH 11.5 solution were heavily corroded and were virtually indistinguishable after salt spray testing.

Figure 8 shows impedance data in Bode magnitude and Bode phase angle plot formats for 2024-T3 surfaces in the three conditions of interest. On a qualitative basis, these spectra can be interpreted using an equivalent circuit (EC) model proposed for damaged porous aluminium oxide surfaces [15–17]. The model accounts for contributions to the spectra from the oxide covered surface and from damage due to pitting in the experimentally accessible portions of the frequency domain.

The selection of the EC model used to fit the EIS data is based in part on the structure of the hydrotalcite coating shown in Fig. 9. This figure shows a cross section of the coating in which the substrate, a dense inner layer, and a porous outer layer can be identified. Figure 10 is an idealized physical representation of the coating showing the two layers of the coating. The model accounts for the

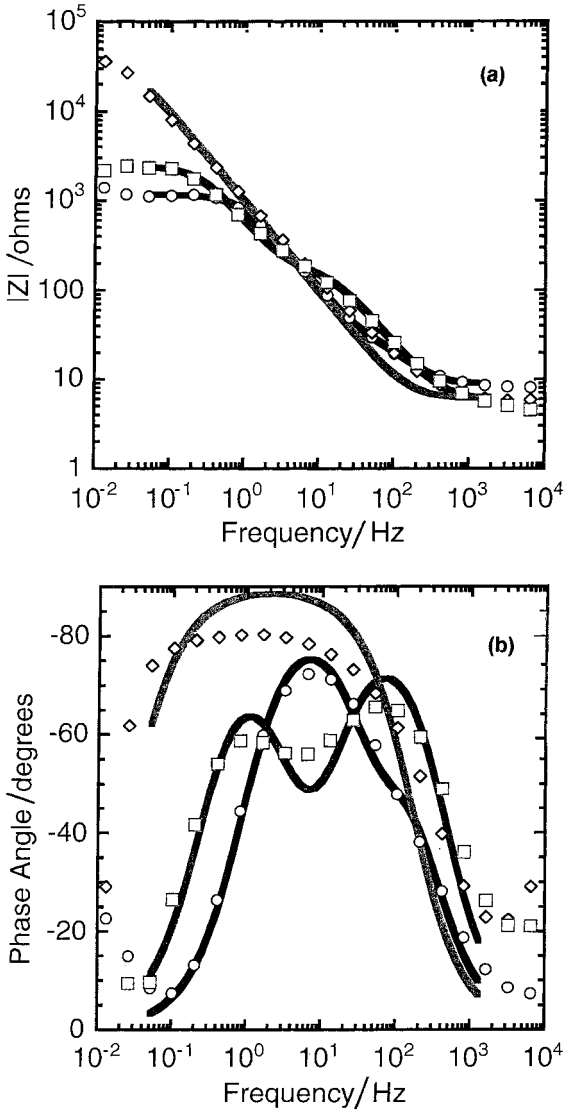

Fig. 8. Bode magnitude (a) and phase angle (b) plots for 2024-T3 surfaces in the three conditions of interest after 24 h of exposure to 0.5 M NaCl. Markers represent EIS data, lines represent the CNLS fit. Key: (○) bare, (◇) pH 11.5 and 13.5, (□) pH 11.5.

presence of pits for situations when damage has occurred. Figure 11 shows an EC model constructed using discrete circuit elements derived from the physical model of Fig. 10.

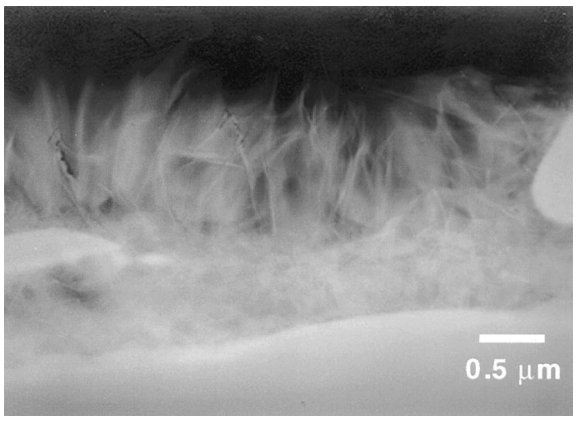

Fig. 9. TEM cross section of the hydrotalcite coating showing two distinguishable layers in the coating.

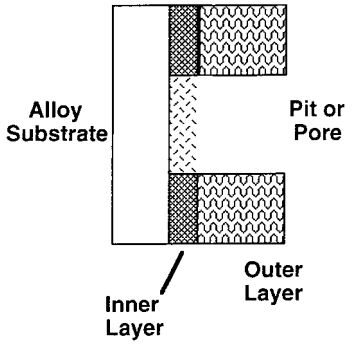

Fig. 10. Idealized physical model of the coating.

In this model, F represents the area fraction of the surface that is pitted. R_{sol} is the solution resistance, R_1 and C_1, and R_2 and C_2 represent resistances and capacitances associated with the two layers of the coating. R_{pit} is a resistance due to the pit solution and R_{corr} and C_{corr} describe the faradaic reactions occurring within the pit. The use of this specific model and the appropriateness of discrete or distributed circuit elements is still the subject of some debate. However, this model is judged to be suitable for the purposes of evaluating relative differences in corrosion resistance among the samples studied here.

In Figure 8 the experimentally determined EIS data are indicated with symbols. The continuous lines indicate the CNLS fit from the EC model. In the Bode magnitude plot, the bare 2024-T3 sample and the one exposed to the pH 11.5 solution exhibit well defined d.c. limits between 1 and $2 \times 10^3\,\Omega$. The plot for the sample exposed to the pH 11.5 and 13.5 solutions exhibits a far more capacitive response and does not reach a well defined d.c. limit at 10^{-2} Hz. In the context of the damage porous aluminium oxide EC model, this response is consistent with a significant amount of damage by pitting for the bare and pH 11.5 samples and little pitting damage for the pH 11.5 and 13.5 sample. Visual observation after testing confirmed this to be the case. The 2024-T3 sample exposed to the pH 11.5 solution exhibits a slightly greater d.c. limit than the bare sample. This response indicates marginally better corrosion resistance compared to bare surfaces. Visual examination

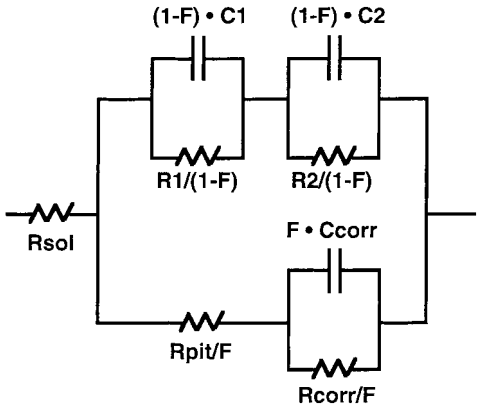

Fig. 11. Generalized equivalent circuit model used to fit EIS data.

showed that this surface was pitted after testing, but suffered noticeably less damage than the bare surface.

Examination of the phase angle plot in Fig. 8 shows that the bare 2024-T3 sample exhibits a single time constant likely due to pitting. In contrast, the sample exposed to the pH 11.5 solution exhibits two discrete time constants, one due to pitting, the other is likely due to the incompletely protective coating. The sample exposed to the pH 11.5 and 13.5 solutions exhibits a broad, somewhat lossy capacitive region.

Values for the circuit elements defined in the EC model are shown in Table 1. The parameters in Table 1 have been normalized by electrode area ($20\,cm^2$), not by fractional area pitted which varied from sample to sample and was not measured. For a surface with a fractional pitted area, F, the elements are solution resistance (R_{sol}), pit electrolyte resistance (R_{pit}/F), pit corrosion resistance (R_{corr}/F), pit capacitance (FC_{corr}). The latter two elements were taken as the primary figures of merit for determining coating corrosion resistance. An explicit accounting of a duplex coating was made by using the two parallel R–C nets comprised of $R_1/(1-F)$, $(1-F)C_1$, $R_2/(1-F)$, and $(1-F)C_2$. However, these elements were not assigned to specific layers of the coating and, as shown in the Table, each element was not always required for a CNLS fit.

The R_{corr}/F value of $3.4 \times 10^4\,\Omega$ cm^2 and FC_{corr} value of $3.9 \times 10^{-4}\,F\,cm^{-2}$ are consistent with pitting corrosion of bare 2024-T3 exposed to an aerated chloride solution. The increase in R_{corr}/F and decrease in FC_{corr} shown in Table 1 indicate a slight decrease in pitting corrosion for the sample exposed to the pH 11.5 solution. However, the sample exposed to both the pH 11.5 and 13.5 solutions exhibits an R_{corr}/F value of $3.4 \times 10^6\,\Omega$ cm^2 indicating high corrosion resistance.

4. Discussion

4.1. *Origin of copper*

In 2024-T3 copper is dissolved in solid solution in the matrix phase of the alloy and is concentrated in to a variety of second phase particles. Predominant particles include $(Al,Cu)_6(Mn,Fe,Cu)$, Al_7Cu_2Fe, $(Al, Cu)_6Mn$, and Al_2CuMg [18]. During surface finishing in extremely alkaline or acid solutions, Cu surface enrichment likely occurs by particle dissolution and dealloying and possible dealloying of the matrix phase. Details of how Cu is extracted and redistributed from noble second phase particles across the surface have not been fully explained, but the phenomenological evidence indicates that the process does occur [19, 20].

Among these second phase particles listed, the Al_2CuMg type should be singled out, because it may contribute significantly to Cu enrichment at surfaces. These particles form during solidification and never fully redissolved in any subsequent thermomechanical processing. Al_2CuMg has been observed to make up 60% of the population of second phase particles 0.5 to 10 μm diameter range [20]. Electrochemical characterization experiments with the compound synthesized in bulk form suggest that it can be electrochemically active with respect to the surrounding microstructure [21].

4.2. *Copper removal by alkaline carbonate solutions*

In terms of corrosion resistance, the primary beneficial effect is derived by exposure to the pH 13.5 solution, but sequential exposure to both solutions must be used to avoid inferior performance. In the pH 11.5 solution, surface oxide formation is rapid and little substrate etching occurs. This coating offers little corrosion resistance, but does suppress etching that would otherwise occur during exposure to the pH 13.5 solution. In this second solution, improved corrosion resistance is developed. Cu is removed from the surface, and the oxide layer is converted to a more protective hydrotalcite coating.

Two factors appear to contribute to the removal of Cu observed during exposure to the pH 13.5 solution. These are: (i) the increased Cu solubility and (ii) the formation of stable cupric carbonate complex that shifts the Cu reduction potential to values more negative than the open circuit potential for the alloy.

Figure 12 shows the total Cu solubility as a function of solution pH [22]. Copper exhibits a solubility minimum at pH 9.8 to 10 where $\log[Cu^{2+}] = -9.48$. For coating solutions in the pH 11.0 to 11.5 range, which is the pH of the first coating bath, the total Cu solubility remains less than 10^{-8} M. Formation of a Cu-rich oxide layer on the alloy surface is not an unexpected phenomenon. However, beyond the solubility minimum, total Cu species solubility increases with increasing pH. At pH 13.5 the Cu solubility increases approximately four orders of magnitude to 2×10^{-4} M.

Table 1. Summary of values obtained from CNLS fitting of EIS spectra

Sample	R_{sol} /Ω	R_{pit}/F /Ω cm^2	R_{corr}/F /Ω cm^2	FC_{corr} /F cm^{-2}	$R_1/(1-F)$ /Ω cm^2	$(1-F)C_1$ /F cm^{-2}	$R_2/(1-F)$ /Ω cm^2	$(1-F)C_2$ /F cm^{-2}
Bare	8.2	0.9×10^3	3.4×10^4	3.9×10^{-4}	7.4×10^4	3.9×10^{-6}	–	–
pH 11.5	5.9	–	1.2×10^5	1.4×10^{-5}	7.7×10^4	2.2×10^{-6}	3.5×10^3	1.5×10^{-6}
pH 11.5 and 13.5	6.1	–	3.4×10^6	4.7×10^{-6}	9.9×10^5	4.2×10^{-6}	–	–

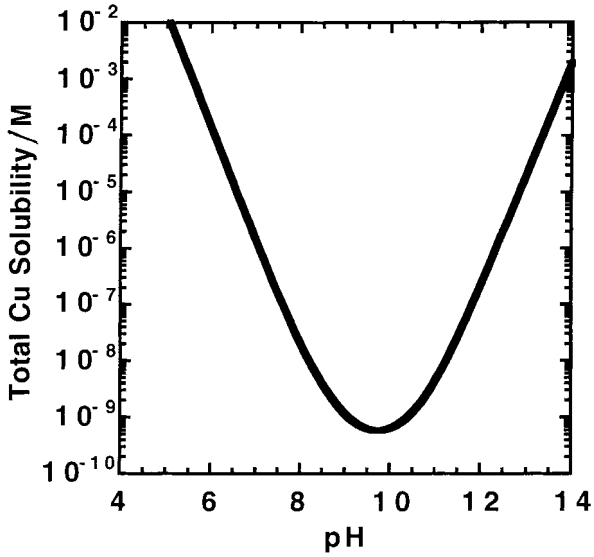

Fig. 12. Total equilibrium Cu solubility as a function of pH computed assuming a CuO-saturated solution and speciation of Cu^{2+} among dominant soluble hydrolysis products [23].

In the carbonate solutions used here, there is an added contribution to Cu solubility by formation of a stable cupric carbonate complex, $Cu(CO_3)_2^{2-}$. This complex forms according to the following reaction [23]:

$$Cu^{2+} + 2CO_3^{2-} \longrightarrow Cu(CO_3)_2^{2-}(aq) \quad (\log K_{form} = 9.83) \tag{1}$$

where K_{form} is the formation constant for the complex. The formation of $Cu(CO_3)_2^{2-}$ increases the ability of these solutions to dissolve and retain Cu from coated surfaces by an additional three orders of magnitude. The magnitude of this effect is estimated by calculating the solubility limit for $Cu(CO_3)_2^{2-}$ in equilibrium with malachite, $Cu(OH)_2(CO_3)$, which is a likely Cu compound in the oxide film formed in the pH 11.5 solution [23]:

$$\left[Cu(CO_3)_2^{2-}\right] = K_{form} \times K_s \times K_{a1} \times K_{a2} = 0.5\,\text{M} \tag{2}$$

where K_{form} is the formation constant from Equation 1, K_s is the solubility product for malachite ($\log K_s = 6.49$), K_{a1} and K_{a2} are the acid dissociation constants for bicarbonate and carbonate ($\log K_{a1} = -6.37, \log K_{a2} = -10.25$).

Redeposition of Cu^{2+} in solution onto the alloy surface is possible but may be restricted in the pH 13.5 solution since the Cu reduction potential is shifted to a value that is equal to or more negative than the measured open circuit potential for the alloy. At pH 13.5 the $Cu/Cu(OH)_2$ reduction potential is given as follows [4]:

$$E_{Cu/Cu(OH)_2} = 0.609 - 0.0591\,\text{pH} = -0.189\,V_{SHE} \text{ or } -0.430\,V_{SCE} \tag{3}$$

The reduction potential is shifted in the negative direction due to $Cu(CO_3)_2^{2-}$ formation by an amount V given by

$$V = 2.303\,(RT/nF)\,\log K_{form} = -0.291\,\text{V} \tag{4}$$

where the gas constant R is $8.31\,\text{J K}^{-1}\,\text{mol}^{-1}$, T is 298 K, n is 2 equiv. mol^{-1}, and Faraday's constant is 96 500 C equiv.$^{-1}$. The corrected $Cu/Cu(OH)_2$ reduction potential becomes $-0.721\,V_{SCE}$ which is negative to the typical open circuit potential for oxide covered 2024-T3 (-0.700 to $-0.500\,V_{SCE}$) [5].

5. Summary

A two stage hydrotalcite coating process involving exposure to a pH 11.5 Li-salt solution followed by exposure to a pH 13.5 solution produces corrosion resistant hydrotalcite films on Al–Cu–Mg alloys. These films are free from Cu in excess of the concentration present in the alloy. Oxide films formed using this method exhibit total impedances greater than $10^6\,\Omega\ \text{cm}^2$ after 24 h exposure to aerated 0.5 M NaCl and withstand 168 h of salt spray exposure without pitting. Cu appears to accumulate in oxide films formed during exposure to pH 11.5 Li-salt solutions, but is subsequently removed when samples are exposed to a pH 13.5 solution due to increased Cu solubility and complexing by carbonate.

Acknowledgements

This work was performed at Sandia National Laboratories sponsored by the US Department of Energy under contract no. DE-AC04-94AL85000. M. Martinez, W. Buttry, B. McKenzie are thanked for their assistance in sample preparation and analysis.

References

[1] J. E. Hatch (Ed.), 'Aluminum: Properties and Physical Metallurgy', ASM, Metals Park, OH (1984) p. 321.
[2] L. F. Modolfo (Ed.), *ibid.*, p. 693.
[3] *Idem*, *ibid.*, p. 254.
[4] M. Pourbaix, 'Atlas of Electrochemical Equilibria in Aqueous Solutions', NACE, Houston, TX (1974) p. 389.
[5] C. A. Drewien and R. G. Buchheit, paper 622, Corrosion '94, NACE, Houston, TX (1994).
[6] N. Fin, H. Dodink, A. E. Yaniv and L. Drori, *Appl. Surf. Sci.* **28** (1987) 11.
[7] J. S. Solomon and N. T. McDevitt, *Thin Solid Films* **84** (1981) 155.
[8] A. V. Pocius, T. H. Wilson, Jr., S. H. Lundquist and S. Sugii, *in* 'Progress in Advanced Materials and Processes: Durability, Reliability and Quality Control (edited by G. Bartelds and R. J. Schekelmann), Elsevier Science, Amsterdam (1985) 71.
[9] T. S. Sun, J. M. Chen and J. D. Venables, *Appl. Surf. Sci.* **1** (1978) 202.
[10] F. Mansfeld and L. Kwiatowski, 'Surface Treatment of High-Cu Aluminum Alloys', University of S. California, Interim Report (1992).
[11] Sanchem 1000, Sanchem, Inc., Chicago, IL.
[12] ZPlot for Windows™, Scribner Associates, Charlottesville, VA.
[13] ASTM B117, Standard Method of Salt Spray (Fog) Testing, v. 3.02, 'Annual Book of ASTM Standards', American Society for Testing and Materials, Philadelphia, PA (1993) 19.
[14] R. G. Buchheit, M. D. Bode and G. E. Stoner, *Corrosion* **50** (1994) 205.

[15] J. Hitzig, K. Juttner and W. J. Lorenz, *J. Electrochem. Soc.* **133** (1986) 887.
[16] F. Mansfeld and M. W. Kendig, *ibid*, **135** (1988) 828.
[17] F. Mansfeld, S. Lin, S. Kim and H. Shih, *Electrochim. Acta* **34** (1989) 1123.
[18] G. Phragmen, *J. Inst. Metals* **77** (1950) 459.
[19] B. Mazurkiewicz and A. Piotrowski, *Corros. Sci.* **23** (1983) 697.
[20] R. G. Buchheit, R. P. Grant, P. F. Hlava, B. A. McKenzie and G. L. Zender, *J. Electrochem. Soc.* **144** (1997) 2621.
[21] K. Urushino and K. Sugimoto, *Corros. Sci.* **19** (1979) 225.
[22] C. F. Baes, Jr. and R. E. Mesmer, 'Hydrolysis of Cations', R. E. Krieger Publishing, Malabar, FL (1986) 268.
[23] P. Schindler, M. Reinert and H. Gamjager, *Helv. Chim. Acta* **51** (1968) 1845.